JMEPEG (2023) 32:7275–7284
https://doi.org/10.1007/s11665-022-07634-2

1059-9495/$19.00

TECHNICAL ARTICLE

Microstructural and Mechanical Investigations of Extruded AlCrFeCoNi/AZ91D Composites

Yongsheng Chen, Lei Wang, and Zesheng Ji

Submitted: 26 April 2022 / Revised: 29 September 2022 / Accepted: 17 October 2022 / Published online: 9 December 2022

This study aimed to investigate the effect of the addition of AlCrFeCoNi particles on the microstructure and mechanical properties of the extruded AlCrFeCoNi/AZ91D composite. We found that the grain size decreases with increasing content of AlCrFeCoNi particles. The micrographs revealed a non-uniform distribution of AlCrFeCoNi particles. In addition, AlCrFeCoNi particles did not decompose nor did it form any kind of reaction layer with the matrix. The strength and hardness of the composite increased simultaneously and the elongation decreased with the increasing content of AlCrFeCoNi particles. The 10 vol.% AlCrFeCoNi/AZ91D composites obtained the best yield strength, ultimate tensile strength, compression strength, hardness, and the worst elongation of 130.2, 319.5, 480.9 MPa, 98.2 HV, and 3.2%, respectively. The improved strength is mainly because of refined grains strengthening and coefficient of thermal expansion (CTE) mismatch strengthening. Simultaneously, the decreased elongation is the result of some particle clusters and stress concentration of interface between AlCrFeCoNi particles and Mg matrix.

Keywords AlCrFeCoNi/AZ91D composites, mechanical properties, microstructure, strengthening mechanism

1. Introduction

In recent years, magnesium alloy matrix composites have gained increasing attention from researchers due to their features like lightweight, high strength-to-weight ratio, and low-cost manufacturing process (Ref 1-4). Although the traditionally reinforced phases (such as SiC, carbon fiber, and Al_2O_3) are still widely used, studies have shown that the mismatch of thermal expansion between traditionally reinforced phases and Mg matrix and their poor wettability lead to undesirable interfacial bonding that limits the improvement in strength (Ref 5-7). Thus, researchers mostly prefer metal particles as the reinforcement with Mg due to their natural interfacial bonding (Ref 8-13).

High-entropy alloy (HEA) has excellent mechanical and physical properties, such as high strength, good plasticity (AlCrFeCoNi HEA: fracture strength-3531 MPa, compression strain -25%), and high-temperature thermal stability (Ref 14-18). Hence, HEA is considered to be a potential candidate reinforcement for metal matrix composites. HEA-reinforced metal composites offer superior properties such as superior wettability, good mechanical properties, and strong interfacial bonding (Ref 19-23). Many research works have explored these properties of HEA/metal composites. As shown in the former literature (Ref 19), we used an rotary blowing stir casting method to fabricate AlCrFeCoNi/AZ91D as-cast composite, AlCrFeCoNi particles are the ideal reinforcement materials to enhance strength and plasticity during casting, and the AlCrFeCoNi hardly reacts with AZ91D matrix to form intermetallic compounds. Lu et al. (Ref 24) prepared CoNiFeCrAl$_{0.6}$Ti$_{0.4}$ particles-reinforced Al matrix composites by using powder technology and hot extrusion, which is a cost-effective approach to eliminate internal pores and improve mechanical properties. They reported the good wettability between CoNiFeCrAl$_{0.6}$Ti$_{0.4}$ and matrix resulting in the enhancement on the strength. Liu et al. (Ref 25) used spark plasma sintering and hot extrusion to prepare AlCrFeCoNi particles-reinforced Cu-based composites. They reported that Cu-rich and CoCrFe-rich FCC structure could improve the interfacial bonding between AlCrFeCoNi and Cu matrix, which can significantly improve the final mechanical properties.

Based on these former researches, it can be seen that the HEA particle has a specific promoting effect on the improvement of matrix mechanical properties. It should be noted that the researchers mostly prefer hot extrusion as the deformation process in the above investigations. Hot extrusion is a process to produce the integral rod materials with fine and uniform microstructures without porosity defects. There are few reports on using hot extrusion method to manufacture HEA/Mg composite rods. In the present paper, AlCrFeCoNi is used as reinforcing particles, and AZ91D magnesium alloy is considered as the matrix. The AlCrFeCoNi/AZ91D composite rods were prepared via hot extrusion process. This study also studied the influence of AlCrFeCoNi particles on the microstructure and mechanical properties of the AZ91D matrix. Further, this study investigated the interface characteristics between the

Yongsheng Chen, School of Materials Science and Engineering, Harbin University of Science and Technology, Harbin, People's Republic of China; and School of Materials Science and Engineering, Heilongjiang University of Science and Technology, Harbin, People's Republic of China; **Lei Wang**, School of Materials Science and Engineering, Heilongjiang University of Science and Technology, Harbin, People's Republic of China; and **Zesheng Ji**, School of Materials Science and Engineering, Harbin University of Science and Technology, Harbin, People's Republic of China. Contact e-mail: jizesheng2022@126.com.

AlCrFeCoNi particles and the AZ91D matrix, and the major strengthening mechanisms.

2. Experimental Method

In this study, commercial brand AZ91D alloy (Al: 8.97 wt.%, Zn: 0.68 wt.%, Mn: 0.17 wt.%, Mg: Bal. wt.%) was used as the matrix material, AlCrFeCoNi particles (purity 99.9%, Al: 8.81, Cr: 20.71, Fe: 23.10, Co: 23.76, Ni: Bal. wt.%) were selected as the reinforcement material, the diameter of AlCrFeCoNi particles is smaller than 25 μm. The as-cast composites specific fabrication process could be found in our previous work (Ref 19). Prior to hot extrusion, the as-cast composites were cut into a cylinder with 60 mm diameter by 58 mm length. The cylinder billets hot-extruded at 400 °C using an extrusion ratio of 16:1. The extrusion speed was set at 2 mm/s. The as-cast AlCrFeCoNi/AZ91D composites with different volume fractions (0, 3, 5, 10 vol.%) were extruded under the same experimental conditions for the purpose of comparison. In addition, AlCrFeCoNi particle content of as-extruded AlCrFeCoNi/AZ91D composites can be estimated by Cr element content. Firstly, the Cr element mass fraction was examined by chemical analysis apparatus (ICP-AES, PQ9100). Secondly, we calculated the AlCrFeCoNi particle mass fraction based the Cr mass fraction. Finally, we convert the mass fraction into the volume fraction. The AlCrFeCoNi particle content of composites with nominal composition of 3, 5, and 10 vol.% as-extruded AlCrFeCoNi/AZ91D composites was analyzed by the above method to obtain 0.15, 0.38, and 0.70 vol.%, respectively. Therefore, the components (0, 3, 5, 10 vol.%) described below are uniform nominal components.

An optical microscope (OM, Carl Zeiss A1) was used to examine the optical microstructure of the specimens. The Image-Pro Plus software v6.0 was used to calculated grain average size. The thermal analysis of the AlCrFeCoNi particles was carried out using differential scanning calorimetry (DSC, Pekin Elmer) at a heating rate of 20 K/min. A scanning electron microscopy (SEM, MX2600FE) equipped with energy-dispersive spectrometer was used to examine the morphologies of the AlCrFeCoNi/AZ91D composites and fracture surfaces. Transmission electron microscopy (TEM) and high-resolution transmission electron microscope (HRTEM Talos 240) were used to identify the morphology of the AlCrFeCoNi particles and the interface between AlCrFeCoNi particles and the Mg matrix. X-ray diffraction (XRD, DX-2700B) with a diffraction angle (2θ) ranging from 10 to 90° was used to perform phase analysis of the composites. A testing machine (Product model INSTRON-5569) was used to conduct room temperature uniaxial tensile test at a velocity of 0.5 mm/min. The tensile specimen size with gage length of 25 and 8 mm in diameter was used as GB228 standards, and each kind of extruded samples was analyzed thrice.

3. Results and Discussion

The XRD spectra are shown in Fig. 1. According to the results of XRD, only α-Mg and β-phase ($Mg_{17}Al_{12}$) were observed in the unreinforced 0 vol.% alloy. The increasing content of AlCrFeCoNi particles highlights the peaks corresponding to AlCrFeCoNi particle phase in the extruded AlCrFeCoNi/AZ91D composites. In addition, no new phase is formed during the hot-extruded procedure, indicating that the AlCrFeCoNi particles do not react with the AZ91D matrix. The DSC curve of the AlCrFeCoNi particles is shown in Fig. 2. Figure 2 shows two obvious exothermic peaks at 1634 K and 1696 K, indicating that the particles have a phase transition during the temperature rise process. However, there is no exothermic peak at 1073 K, indicating that the AlCrFeCoNi particles have high thermodynamic stability at 1073 K.

Figure 3 shows the microstructures of as-extruded AlCrFeCoNi/AZ91D composites (perpendicular to the extrusion direction). Figure 3(a) shows equiaxed grains, while Fig. 3(b), (c), and (d) shows dynamic recrystallization (DRX) grains and necklace-like black particles along the grain boundaries. The average grain size (seen in Fig. 3e), measured using the mean linear intercept method, is approximately 29.1 μm for as-extruded AZ91D. With the addition of AlCrFeCoNi particles to 3, 5, and 10 vol.% composites, the corresponding average size of the α-Mg grains decreased to 21.8, 19.5, and 17.3 μm,

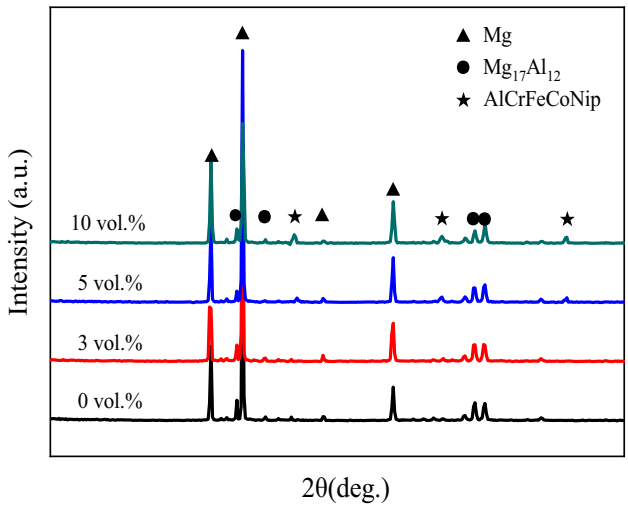

Fig. 1 XRD spectra of as-extruded AlCrFeCoNi/AZ91D composites

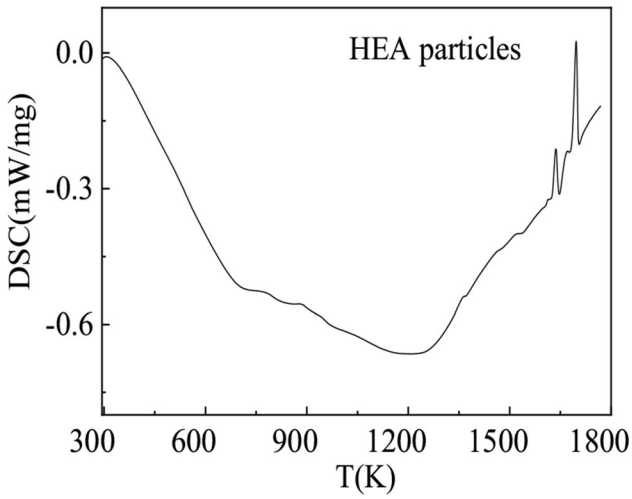

Fig. 2 DSC curve of the AlCrFeCoNi particles

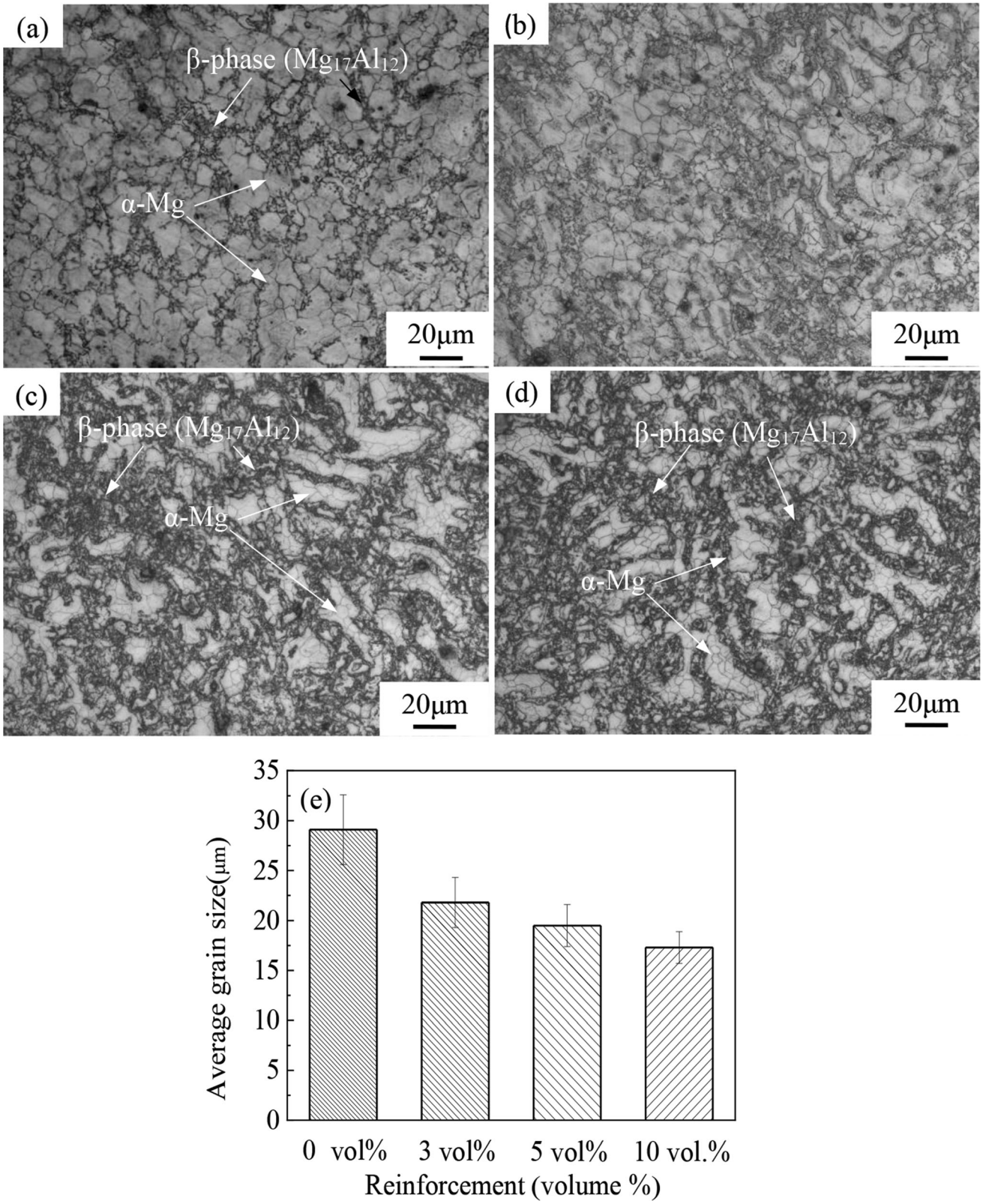

Fig. 3 Optical microstructure on cross sections of as-extruded AlCrFeCoNi/AZ91D composites (vol.%) from perpendicular to the extrusion direction: (a) 0 HEA, (b) 3 HEA, (c) 5 HEA, (d) 10 HEA, and (e) average grain size, perpendicular to the extrusion direction

respectively. This indicates the effectiveness of AlCrFeCoNi particles in restricting the growth of DRXed grains by the pinning effect. Therefore, AlCrFeCoNi particles have potential applications in refining the grain of composites.

Figure 4 shows the SEM micrograph of as-extruded AlCrFeCoNi/AZ91D composites. The EDS patterns of points A and B (marked in Fig. 4a) are shown in Fig. 4(b) and (c), respectively, indicating that the black phase and long strip-

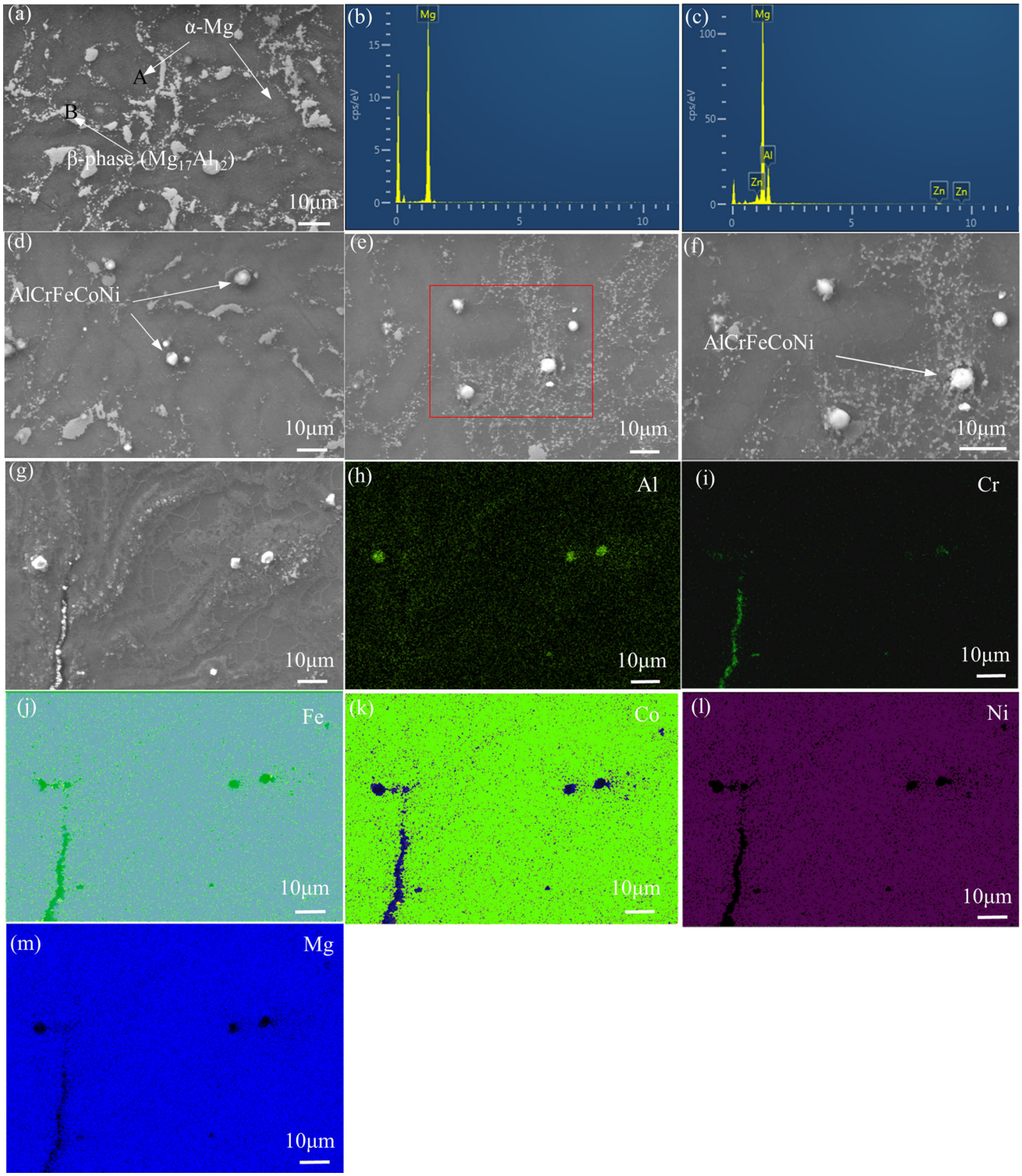

Fig. 4 SEM images on cross sections of as-extruded AlCrFeCoNi/AZ91D composites (vol.%): (a) 0 HEA, (b) EDS analysis of point A, (c) EDS analysis of point B, (d) 3 HEA, (e) 5 HEA, (f) high magnification of (e), (g) 10 HEA, (h-m) EDS mapping results of (g)

shaped phase were confirmed as α-Mg and β-phase ($Mg_{17}Al_{12}$). The magnified zone marked in Fig. 4(e) by the red dotted box can be observed in Fig. 4(f) The strip shape clusters of AlCrFeCoNi particles appear in 10 vol.% samples (marked in Fig. 4g), and its mapping element distributions are given in Fig. 4(h), (i), (j), (k), (l), and (m). Thus, the bright, gray, and dark regions in Fig. 4(d), (e), (f), and (g) correspond to AlCrFeCoNi particles, β-phase ($Mg_{17}Al_{12}$) and α-Mg in the composites. The content of AlCrFeCoNi particles significantly affects the morphology and size of β-phase ($Mg_{17}Al_{12}$) and α-Mg. As the volume fraction of AlCrFeCoNi particles increased from 0 to 10%, the β-phase ($Mg_{17}Al_{12}$) and α-Mg size

decreased, smaller grain size is obtained in the 10 vol.% composites. Thus, this indicates that the AlCrFeCoNi particles could effectively refine the matrix.

Figure 5 shows the TEM characterization of the as-extruded AlCrFeCoNi/AZ91D composites. As shown in Fig. 5(a) and (b), a clear boundary exists between the AlCrFeCoNi particle and α-Mg. The results of the line scan suggest the absence of reactants and element diffusion layer at the interface of AlCrFeCoNi/α-Mg. Figure 5(c) shows the intact AlCrFeCoNi particle and numerous dislocations stacking around the AlCrFeCoNi particle, and the selected-area electron diffraction patterns (SADPs) of AlCrFeCoNi particle is shown in the insets of Fig. 5(c), it is visible from inset that the AlCoCrFeNi particle has a BCC structure. The combined results of Fig. 4 and 5 suggest that the hot extrusion preparation process causes no damage to the AlCrFeCoNi particle. The HRTEM image of AlCrFeCoNi particle and α-Mg matrix is shown in Fig. 5(d) This shows AlCrFeCoNi particle bonds well with α-Mg matrix because the interface between AlCrFeCoNi particle and α-Mg matrix is flat and clear without reaction layers. It can be concluded that the AlCrFeCoNi was tightly bonded with the α-Mg matrix. Indeed, different thermal expansion coefficients result in some dislocations around the AlCrFeCoNi particle during hot extrusion cooling. The AlCrFeCoNi particle and AZ91D matrix have different deformation abilities. The AlCrFeCoNi particle hindered matrix deformation, which resulted in more stress concentrations around the AlCrFeCoNi particle and eventual accumulation of dislocations during the hot extrusion process. Therefore, the above results highlight the mechanical property of the as-extruded AlCrFeCoNi/AZ91D composites.

Typical tensile curves of as-extruded AlCrFeCoNi/AZ91D samples could be observed in Fig. 6. The values of compression strength (UCS), yield strength (YS), ultimate tensile

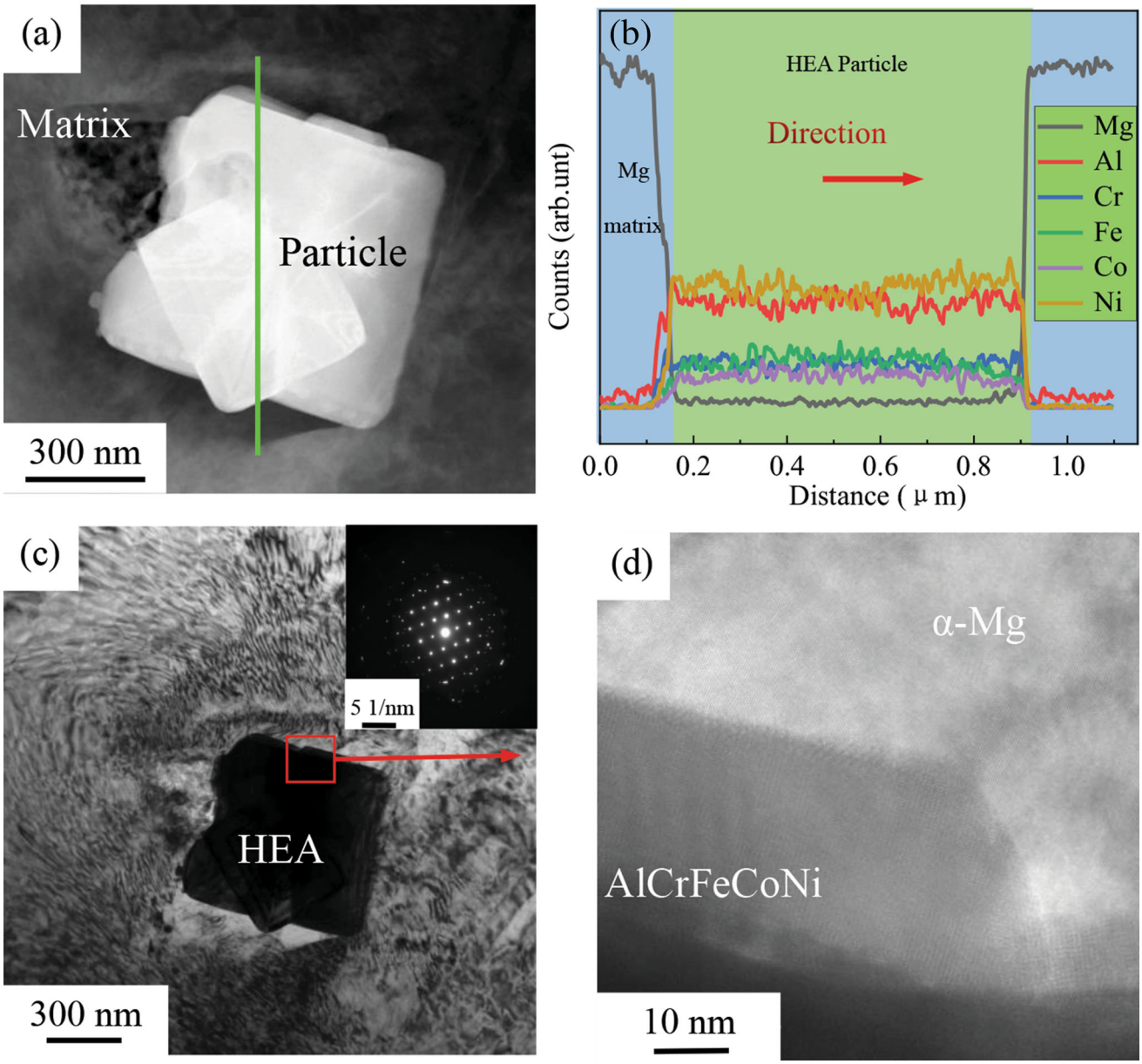

Fig. 5 TEM and HRTEM images of as-extruded AlCrFeCoNi/AZ91D composites (a) AlCrFeCoNi particle, (b) linear scanning result of (a), (c) dislocation stacking in the matrix, (d) HRTEM image in (c)

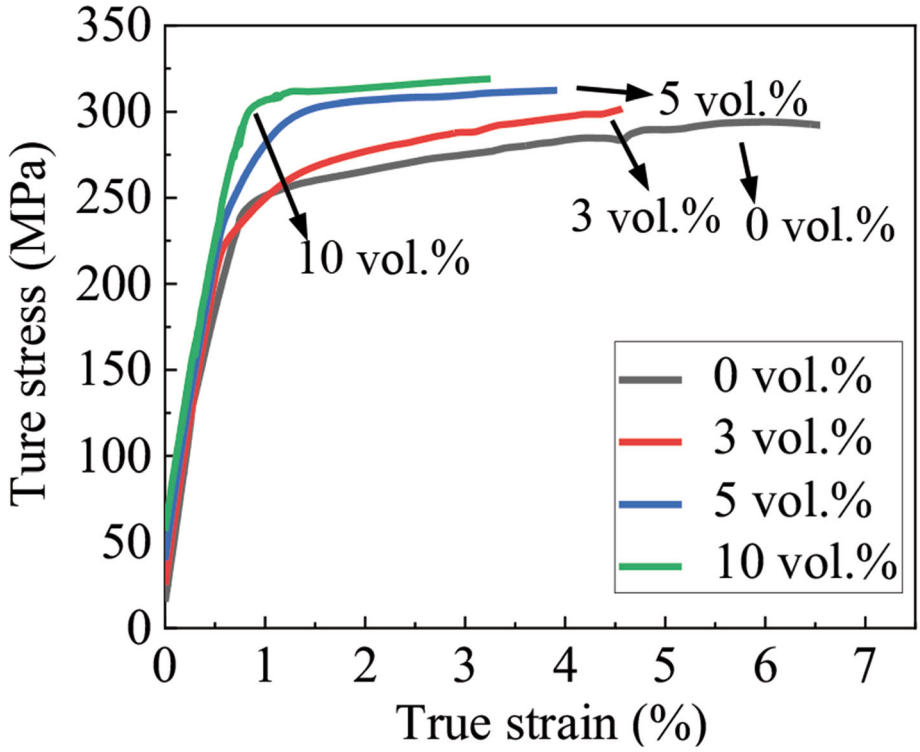

Fig. 6 As-extruded tensile strain–stress curves

Table 1 Summary of the mechanical properties of sample composites

Materials	Mechanical properties				
	UCS, MPa	0.2%YS, MPa	UTS, MPa	Elongation, %	Microhardness, HV
0 vol.%	453.9 ± 10.6	97.3 ± 12.9	294.3 ± 10.5	6.6 ± 0.9	79.9 ± 1.2
3 vol.%	465.7 ± 6.5	104.5 ± 3.5	301.4 ± 5.6	4.5 ± 0.6	88.1 ± 2.8
5 vol.%	475.8 ± 5.6	117.1 ± 3.8	310.2 ± 4.2	3.8 ± 0.4	94.2 ± 2.4
10 vol.%	480.9 ± 4.1	130.2 ± 5.6	319.5 ± 2.4	3.2 ± 0.4	98.2 ± 3.8

strength (UTS), elongation and hardness of as-extruded AlCrFeCoNi/AZ91D samples are also summarized in Table 1. The strength and hardness of composites increase with increasing AlCrFeCoNi particle content. Even though the 10 vol.% sample has inhomogeneous distribution of AlCrFeCoNi particles, it exhibited the maximal strength and hardness value. The maximum UCS, YS, UTS, and hardness values were 480.9, 130.2, 319.5, and 98.2 HV, respectively. Due to the relatively high hardness of AlCrFeCoNi particle (520 HV), numerous AlCrFeCoNi particles exist in the AZ91D matrix. In addition, the average grain size of the composites decreases with increasing AlCrFeCoNi particle content. As a result, the introduction of AlCrFeCoNi particle and grain refinement are responsible for hardness enhancement. However, the as-extruded AlCrFeCoNi/AZ91D composites exhibit elongation inferior to the as-extruded AZ91D sample. In this case, the increase in the content of AlCrFeCoNi particles from 0 to 10 vol.% results in a decrease in the elongation from 6.6 to 3.2%. The overall decrease in the elongation of AZ91D by 51.5% cannot be improved by introducing AlCrFeCoNi particles. This is because the poor elongation is mainly caused by the dislocation pile-up around the AlCrFeCoNi particles, which results in stress concentration and weakened interfacial bonding. Consequently, crack initiation and propagation between AlCrFeCoNi and α-Mg matrix are observed. Furthermore, the agglomeration of AlCrFeCoNi particles leads to the debonding of AlCrFeCoNi particles and Mg matrix, which results in a decrease in the ductility of composites. Therefore, our findings indicate that simultaneous increase in both strength and elongation for the as-extruded AlCrFeCoNi/AZ91D composites is difficult to attain.

Lu et al.'s work (Ref 24) illustrated that AlCrFeCoNi particles resulted in significant decrease in ductility and increase in strength of HEA/Al composites during extrusion. The tensile strength of as-extruded AlCrFeCoNi/AZ91D composite is also increased because of the effect of grain refinement, stress transfer, and CTE mismatch. The Orowan effect on the strengthening of as-extruded AlCrFeCoNi/AZ91D composite should also be taken into consideration. With the increase in the content of AlCrFeCoNi particle in as-extruded AZ91D composites, grain refinement becomes more noticeable. In other words, the smaller the grain size, the stronger is the

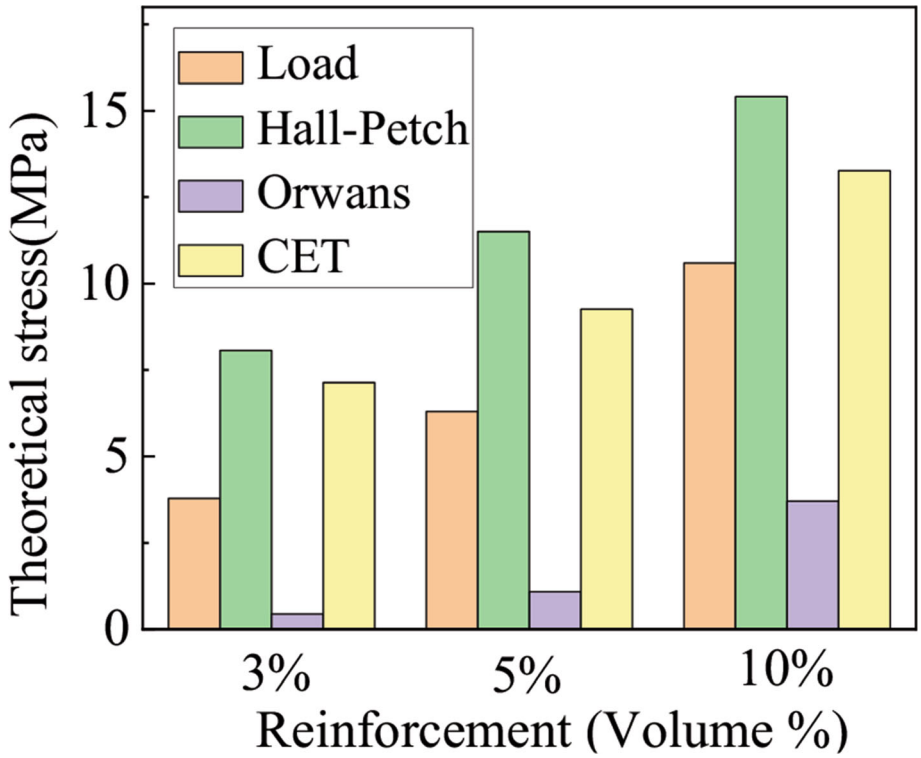

Fig. 7 The calculated contribution of different strengthening effect of composites

grain refining effect. According to the above microstructural observation and analysis, the grain refinement is mainly ascribed to stimulated DRX and restricted growth of DRXed grains by the AlCrFeCoNi particles. A higher dislocation density promotes the recrystallization nucleation of Mg matrix grains. Meanwhile, the AlCrFeCoNi particles act as strong obstacles to the dislocation movement, which will restrict the further growth of DRXed grains by pinning the grain boundary. Thus, the effect of grain refinement on strength can be estimated using the Hall–Petch formula (Ref 26):

$$\Delta\sigma_{Hall-Petch} = k(d_{\text{composites}}^{-1/2} - d_{\text{AZ91D}}^{-1/2}) \quad \text{(Eq 1)}$$

In the above equation, d is the average grain size, $d_{\text{AZ91D}} = 29.1\ \mu\text{m}$ (Ref 21); k is the Hall–Petch coefficient, and its value is 280 MPa $\mu\text{m}^{1/2}$.

The strong interfacial bonding facilitates the transfer of more shear stress from the as-extruded AZ91D matrix to AlCrFeCoNi particle. This also increases the strength of the composite. The stress transfer effect of AlCrFeCoNi particle can be expressed as Ref 19:

$$\Delta\sigma_{load} = 1.5V_p\sigma_i \quad \text{(Eq 2)}$$

where V_{p} is the volume fraction of AlCrFeCoNi particle in matrix and σ_i is strength of as-extruded AZ91D matrix.

Following the hot extrusion process, dislocation usually forms around AlCrFeCoNi particles in the matrix under air cooling (see Fig. 5). This is because of the difference mismatch between Mg matrix and AlCrFeCoNi. The thermal mismatch would favor strength, and its effect can be determined using below equation (Ref 24):

$$\Delta\sigma_{\text{CTE}} = \sqrt{3}\alpha\text{Gb}\sqrt{\frac{12V_p\Delta C\Delta T}{(1-V_p)\text{b}d_p}} \quad \text{(Eq 3)}$$

where α is a constant having the value of 1.25. G is the shear modulus (Mg matrix) of 16.6 GPa, and b is the Burgers vector (Mg matrix) of 32.1 nm. ΔC refers to the difference in CTE between AlCrFeCoNi and Mg matrix. ΔT is D-value between hot extrusion and room temperature. dp refers to the diameter of AlCrFeCoNi particle.

AlCrFeCoNi particles in AZ91D matrix can hinder dislocation movement, but the strength of extruded AlCrFeCoNi/AZ91D composite is improved due to the Orowan effect. This effect can be measured using the below equation (Ref 26):

$$\Delta\sigma_{\text{Orowan}} = \frac{\varphi Gb}{d_p}\left(\frac{6V_{\text{p}}}{\pi}\right) \quad \text{(Eq 4)}$$

where G, b, d_{p}, and V_{p} are the same as defined earlier and φ is a constant equal to 2.

As mentioned above, the theoretical strength of composites can be written as:

$$\Delta\sigma = \sigma_{Hall-Petch} + \sigma_{\text{CET}} + \sigma_{load} + \sigma_{Orowan} \quad \text{(Eq 5)}$$

Figure 7 shows the results of the above four strengthening mechanisms calculated by Eq 1-4. In the present work, the main strengthening mechanisms were grain refinement and CTE mismatch. However, the stress transfer and Orowan effect were not dominant due to the clustered AlCrFeCoNi particles.

Figure 8(a), (c), (e), and (g) shows macroscopic morphologies of the 0%, 3 vol.%, 5 vol.%, and 10 vol.% as-extruded AlCrFeCoNi/AZ91D samples, respectively. Correspondingly,

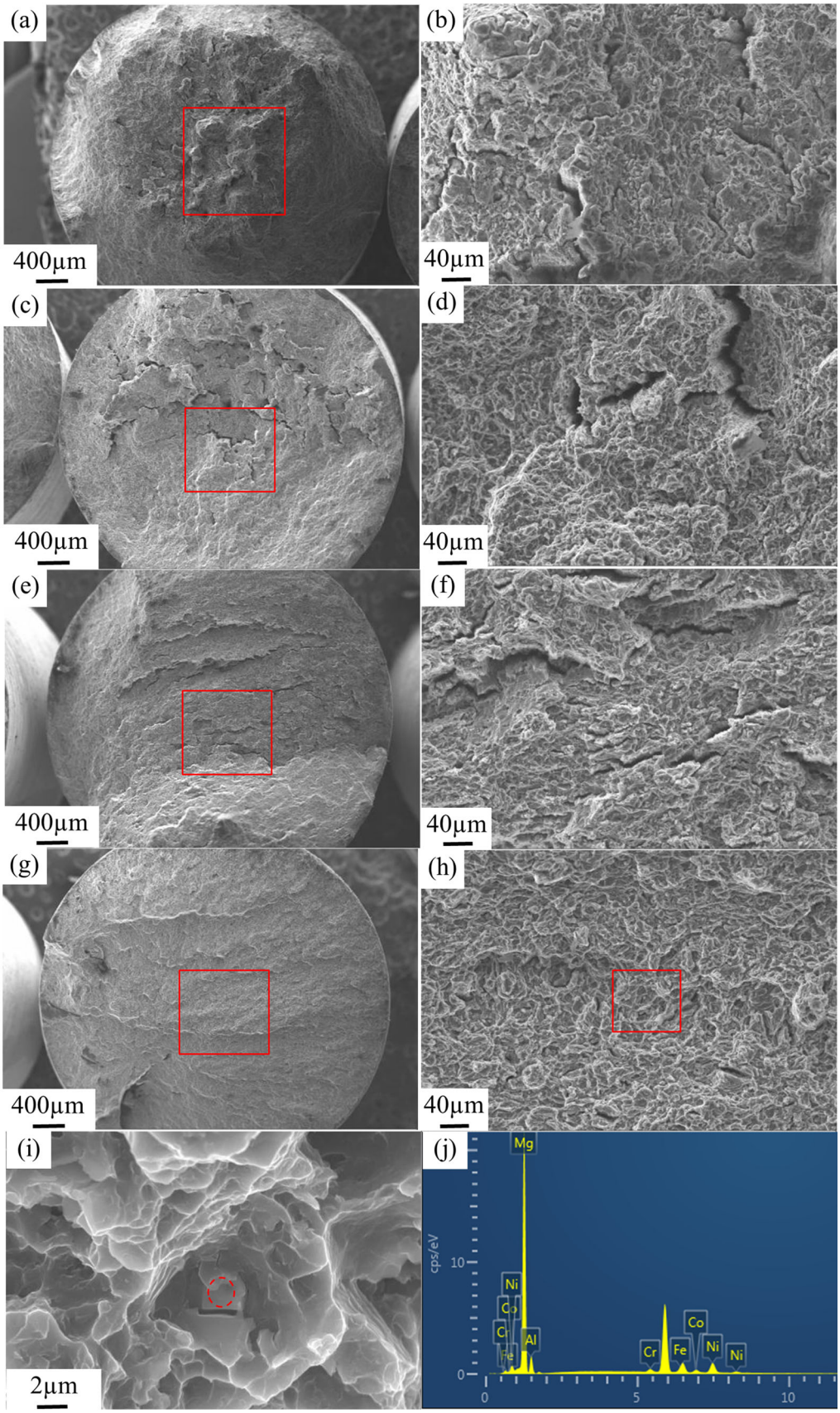

Fig. 8 Fracture surfaces of as-extruded AlCrFeCoNi/AZ91D composites (vol.%): (a, b) 0 HEA, (c, d) 3 HEA, (e, f) 5 HEA, (g, h) 10 HEA, (i) is the corresponding magnified image in (h), and its EDS of AlCrFeCoNi particle is shown in (j)

Fig. 8(b), (d), (f), and (h) presents the high-magnification morphologies in the red frame. Figure 8(i) is the corresponding magnified image in Fig. 8(h), and its EDS of AlCrFeCoNi particle is shown in Fig. 8(j). With the increasing content of AlCrFeCoNi particles, the surface of tensile fracture becomes flat and smooth. Some dimples were observed on the fracture surfaces of the 0% sample, implying its good ductility. This indicates that the 0% sample possesses a mixed fracture of toughness and brittleness mode. In Fig. 8(c), (d), (e), (f), (g), and (h), the as-extruded AlCrFeCoNi/AZ91D exhibits brittle fracture structure. Besides, Fig. 8(i) shows the propagation of cracks around AlCrFeCoNi particles. In other words, the clustered AlCrFeCoNi particles and stress concentration are prone to the induced interfacial debonding between the AlCrFeCoNi particles and α-Mg matrix during tensile testing. Therefore, the increase in the content of AlCrFeCoNi particles causes a reduction in the ductility of composites.

4. Conclusion

(1) With the addition of AlCrFeCoNi particles (0, 3, 5, and 10 vol.%), the grain size of as-extruded AlCrFeCoNi/AZ91D composites was significantly reduced through the pinning effect of AlCrFeCoNi particles. The 10 vol.% composites exhibited the agglomeration of AlCrFeCoNi particles, which were well bonded with the matrix due to the absence of diffusion layer and element reactions.
(2) The increasing content of AlCrFeCoNi particles results in the higher strength and hardness of composites. The 10 vol.% composite attained YS, UTS, UCS and hardness of 130.2, 319.5, 480.9, and 98.2 HV. This improved strength is mainly attributed to the fine-grained strengthening and CTE mismatch strengthening.
(3) The AlCrFeCoNi particle content affects the elongation of the composite. When the particle content increases from 0 to 10 vol.%, the decreased elongation is mainly due to the agglomeration of particles and stress concentration.

Funding

This work was supported by the University Nursing Program for Young Scholars with Creative Talents in Heilongjiang Province (UNPYSCT-2020033) and National Natural Science Foundation of China (No. 51574100).

References

1. K. Wu, M.Y. Zheng, C.K. Yao, T. Sato, H. Tezuka, A. Kamio, and D.X. Li, Crystallographic Orientation Relationship Between SiCw and Mg in Squeeze-Cast SiCw/Mg Composites, *J. Mater. Sci. Lett.*, 1999, **18**, p 1301–1303.
2. C.L. Zhang, X.J. Wang, X.M. Wang, X.S. Hu, and K. Wu, Fabrication, Microstructure and Mechanical Properties of Mg Matrix Composites Reinforced by High Volume Fraction of Sphere TC4 Particles, *J. Magnes. Alloy.*, 2016, **4**, p 286–294.
3. Q.H. Yuan, G.H. Zhou, L. Liao, Y. Liu, and L. Luo, Interfacial Structure in AZ91 Alloy Composites Reinforced by Graphene Nanosheets, *Carbon*, 2018, **127**, p 177–186.
4. W.B. Yu, X.J. Wang, H.B. Zhao, C. Ding, Z.Y. Huang, H.X. Zhai, Z.P. Guo, and S.M. Xiong, Microstructure, Mechanical Properties and Fracture Mechanism of Ti_2AlC Reinforced AZ91D Composites Fabricated by Stir Casting, *J. Alloy. Compd.*, 2017, **702**, p 199–208.
5. L.F. Yi, T. Yamamoto, T. Onda, and Z.C. Chen, Orientation Control of Carbon Fibers and Enhanced Thermal/Mechanical Properties of Hot-Extruded Carbon Fibers/Aluminum Composites, *Diam. Relat. Mater.*, 2021, **116**, p 108432.
6. X.F. Niu, G. Li, Z.Y. Zhang, P.W. Zhou, H.X. Wang, S.X. Zhang, and W.L. Cheng, Simultaneously Improving the Strength and Ductility of Extruded Bimodal Size SiCp/AZ61 Composites: Synergistic Effect of Micron/Nano SiCp and Submicron Mg17Al12 Precipitates, *Mater. Sci. Eng. A*, 2019, **743**, p 207–216.
7. Q.H. Yuan, X.S. Zeng, Y. Liu, L. Luo, J.B. Wu, Y.C. Wang, and G.H. Zhou, Microstructure and Mechanical Properties of AZ91 alloy Reinforced by Carbon Nanotubes Coated with MgO, *Carbon*, 2016, **96**, p 843–855.
8. I.W. Hall, G.R. Brewer, and A. Magata, Fracture Toughness of Thermally Cycled α-Al_2O_3/Mg Alloy Metal Matrix Composites, *J. Mater. Sci. Lett.*, 1989, **8**, p 343–345.
9. L. Wang, Y.C. Feng, L.P. Wang, Y.H. Chen, and E.J. Guo, Effect of Al on Grain Refinement and Mechanical Properties of Mg-3Nd Casting Alloy, *J. Mater. Eng. Perform.*, 2018, **27**, p 2099–2109.
10. A.R. Salasel, A. Abbasi, N. Barri, H. Mirzadeh, M. Emamy, and M. Malekan, Effect of Si and Ni on Microstructure and Mechanical Properties of In-situ Magnesium-Based Composites in the As-Cast and Extruded Conditions, *Mater. Chem. Phys.*, 2019, **232**, p 305–310.
11. I. Dinaharan, S. Zhang, G.Q. Chen, and Q.Y. Shi, Titanium Particulate Reinforced AZ31 Magnesium Matrix Composites with Improved Ductility Prepared Using Friction Stir Processing, *Mater. Sci. Eng. A*, 2020, **772**, p 138793.
12. A.A. Shayanpoor and H.R.R. Ashtiani, Microstructural and Mechanical Investigations of Powder Reinforced Interface Layer of Hot Extruded Al/Cu Bimetallic Composite Rods, *J. Manuf. Process.*, 2022, **77**, p 313–328.
13. H. Yu, H.P. Zhou, Y. Sun, L.L. Ren, Z.P. Wan, and L.X. Hu, Microstructures and Mechanical Properties of Ultrafine-Grained Ti/AZ31 Magnesium Matrix Composite Prepared by Powder Metallurgy, *Adv. Powder Technol.*, 2018, **29**, p 3241–3249.
14. Z.W. Yuan, W.B. Tian, F.G. Li, Q.Q. Fu, X.G. Wang, W.F. Qian, and W.C. An, Effect of Heat Treatment on the Interface of High-Entropy Alloy Particles Reinforced Aluminum Matrix Composites, *J. Alloy. Compd.*, 2020, **822**, p 153658.
15. Y. Zhang, X.Q. Li, H. Gu, R.Q. Li, P.H. Chen, C.L. Kong, and H.L. Yu, Insight of High-Entropy Alloy Particles-Reinforced 2219 Al Matrix Composites Via the Ultrasonic Casting Technology, *Mater. Charact.*, 2021, **182**, p 111548.
16. J.C. Li, Y.L. Li, F.F. Wang, X.C. Meng, L. Wan, Z.B. Dong, and Y.X. Huang, Friction Stir Processing of High-Entropy Alloy Reinforced Aluminum Matrix Composites for Mechanical Properties Enhancement, *Mater. Sci. Eng. A*, 2020, **792**, p 139755.
17. J.C. Gao, X. Wang, S.Y. Zhang, L. Yu, J.F. Zhang, and Y.F. Shen, Producing of FeCoNiCrAl High-Entropy Alloy Reinforced Al Composites Via Friction Stir Processing Technology, *Int. J. Adv. Manuf. Tech.*, 2020, **110**, p 569–580.
18. Y.Q. Zhang, D.D. Wang, and S.Y. Wang, High-Entropy Alloys for Electrocatalysis: Design, Characterization, and Applications, *Small*, 2022, **18**, p 2104339.
19. Y.S. Chen, Z.S. Ji, M.L. Hu, and H.Y. Xu, Microstructure and Mechanical Properties of AlCrFeCoNi High-Entropy Alloy Particle Reinforced Mg-9Al-1Zn Matrix Composites, *Int. J. Mater. Res.*, 2021, **112**, p 538–545.
20. K.G. Luo, H.Q. Xiong, Y. Zhang, H. Guan, Z.D. Lian, C.L. Kong, and H.L. Yuan, AA1050 Metal Matrix Composites Reinforced by High-Entropy Alloy Particles Via Stir Casting and Subsequent Rolling, *J. Alloy. Compd.*, 2022, **893**, p 162370.
21. W.P. Chen, Z.X. Li, T.W. Lu, T.B. He, R.K. Li, B. Li, B.B. Wan, Z.Q. Fu, and S. Scudino, Effect of Ball Milling on Microstructure and

Mechanical Properties of 6061Al Matrix Composites Reinforced with High-Entropy Alloy Particles, *Mater. Sci. Eng A*, 2019, **762**, p 138116.
22. Z.W. Yuan, H. Liu, Z. Ma, X.K. Ma, K. Wang, and X.M. Zhang, Microstructure and Properties of High Entropy Alloy Reinforced Titanium Matrix Composites, *Mater. Charact.*, 2022, **187**, p 111856.
23. C. Ding, K.P. Yu, H.R.J. Nodooshan, S.L. Ye, and P. Yu, Effect of Powder Microstructure on the Thermal and Mechanical Properties of Hot Extruded Al-CNT Composite, *J. Alloy. Compd.*, 2022, **891**, p 162059.
24. T.W. Lu, W.P. Chen, Z.X. Li, T.B. He, B. Li, R.K. Li, Z.Q. Fu, and S. Scudino, Processing and Mechanical Properties of Fine Grained Al Matrix Composites Reinforced with a Uniform Dispersion of Nanocrystalline High-Entropy Alloy particles, *J. Alloy. Compd.*, 2019, **801**, p 473–477.
25. Y.Z. Liu, J. Chen, Z. Li, X.H. Wang, P. Zhang, and J.N. Liu, AlCoCrFeNi High Entropy Alloy Reinforced Cu-Based Composite with High Strength and Ductility After Hot Extrusion, *Vacuum*, 2021, **184**, p 109882.
26. J.L. Ye, J.B. Li, H. Luo, J. Tan, X.H. Chen, B. Feng, K.H. Zheng, and F.S. Pan, Effect of Micron-Ti Particles on Microstructure and Mechanical Properties of Mg-3Al-1Zn Based Composites, *Mater. Sci. Eng. A*, 2022, **833**, p 142526.